Combined Atmospheric and Air-water Interface Correction for Waterquality Estimations

Peter A. Keller and Klaus I. Itten

Remote Sensing Laboratories, RSL
University of Zurich, Winterthurerstrasse 190, CH-8057 Zurich
pkeller@geo.unizh.ch

Key Words: water quality, atmospheric correction, air-water interface, imaging spectroscopy

Abstract

An extension of the atmospheric correction model ATCOR 4 is presented for the pre-correction of inland water. In this study, the visibility is obtimized under the assumption that the water-leaving radiance is zero in the near infrared (dark target approach) leading to a pixel based correction. A sensitivity analysis is performed with respect to the retrieval of chlorophyll *a*. It is shown that the assumptions made for the pre-correction is crucial for the relative and absolute lake water constituent concentration.

1. Introduction

The emphasis of this study is put on the determination the influence of unknown atmospheric parameters on the determination of lake quality parameter (i.e., chlorophyll a *CHL*). The generation of a concentration map includes three major steps: (i) atmospheric correction, (ii) interface correction, and (iii) determination of the concentration. For these purposes, empirical or analytical methods can be used. The former have the advantage that the calculation are performed in an easy and fast way, the later that the results can be generalized. However, analytical models need different parameters which are not *a priori* known. In general, operational methods are based on both, educated guesses and measured information, since the amount of unknown parameters does not allow the determination of each parameter.

In this study a combined atmospheric and air-water interface correction is presented. For the verification of the method, a CASI scene flown over the pre-alpine Lake Zug (38 km^2) on August 10, 1997, is used. Chlorophyll *a* maps were generated based on the corrected data.

2. Methods

2. 1 ATCOR 4 /MODTRAN 4

ATCOR 4 is a program designed for the atmospheric correction of airborne imaging spectrometer data (Richter, 1999). The original algorithm allows the consideration of the external (x, y, z) and internal (roll, pitch, yaw) position of the aeroplane; in the rewriting of the algorithms, this feature is not included.

According to Kaufman and Sendra (1988), the radiative transfer equation can be written as:

$$L_{sensor}(\lambda) = L_{path}(\lambda) + \frac{\rho(\lambda)}{\pi}\tau(\lambda)E_g(\lambda, \rho_r), \tag{1}$$

where L_{sensor} is the at-sensor radiance for surface reflectance ρ, L_{path} the path radiance, τ the total (direct and diffuse) ground-to-sensor transmittance, ρ_r the reference background reflectance, and E_g the global flux on a horizontal surface (i.e., the sum of direct and diffuse flux). E_g depends on the background reflectance:

$$E_g(\lambda, \rho_r) = \frac{E(\lambda, \rho = 0)}{1 - \rho_r(\lambda)s(\lambda)} = \frac{E_{dir}(\lambda) + E_{dif}(\lambda, \rho = 0)}{1 - \rho_r(\lambda)s(\lambda)}. \tag{2}$$

The spherical albedo of the atmosphere s accounts for atmospheric backscattering to the ground. Assuming constant reflectance for each channel of a spectrometer, Eq. 1 and Eq. 2 are also valid for quantities convolved to the spectral band response function; the broader the response function, the larger the introduced error. For water applications, this is especially a problem at the chlorophyll absorption maximum at 675 nm. Of course the reflectances ρ and ρ_r are not known before the correction and must therefore be determined iteratively.

The correction involves three steps. First, Eq. 1 is solved for ρ neglecting the influence of the adjacency effect:

$$\rho^{(1)} = \frac{\pi(d^2 L_{sensor} - L_{path})}{\tau E_g(\rho_r = 0.15)}, \tag{3}$$

where $E_g(\rho_r = 0.15)$ is the global flux evaluated for a reference background of $\rho_r = 0.15$. The parameter d is the sun-earth distance (astronomical units) for the date of image acquisition. The factor d^2 scales the measured signal since path radiance and the global flux are calculated for $d = 1$.

Secondly, the adjacency effects are corrected, and thirdly, the atmospheric albedo of the global flux is included which was initially calculated for $\rho_r = 0.15$.

For the determination of the terms of Eq. 1 to Eq. 3, MODTRAN 4 is used (Berk et al., 1989) which requires environmental parameters (ground altitude, sun azimuth and zenith angle), flight parameters (flight altitude and heading of the aircraft), sensor specific parameters (centre wavelength, FWHM, view angle), and atmospheric parameters (visibility, atmospheric and aerosol model) for the calculations.

2. 2 Air-water Interface

The air-water interface transfer can be summarized with (Mobley, 1994):

$$R_{Rs}(a;\xi) = \frac{t(w, a;\xi' \rightarrow \xi)t(a, w)}{n_w^2(1 - R(w)r(w, a))}\frac{R(w)}{Q} + r(a, w;\xi) \text{ [sr}^{-1}\text{]}. \tag{4}$$

This equation takes into account the surface reflection of downwelling irradiance $r(a, w;\xi)$, the transfer of the downwelling irradiance into the waterbody $t(a, w)$, the internal reflection of the upwelling radiance at the interface $r(w, a)$, and the transfer of upwelling radiance across the interface $t(w, a;\xi' \rightarrow \xi)/n_w^2$. The first term in the brackets describes the origin of the radiation (a = air, w = water), the second term where the radiation is pointing to, ξ is the viewing zenith angle in air, and ξ' the corresponding angle in water.

The description of the transfer functions of the downwelling radiation is done after Bukata et al. (1995) who distinguish different transfer functions for sunlight and diffuse skylight. This is reasonable as the higher the rate of diffuse light, the higher the average of the incidence zenith angles, the higher the surface reflection and the smaller the transfer across the interface.

Modellings (Fig. 1) show that:

- The transfer functions $t(a, w)$ and $t(w, a;\xi' \rightarrow \xi)$ only depend weakly (or not at all) on wavelength and visibility; the variations are only about 1-2%. Thus both parameters can be assumed to be constant for the calculations.
- On the other hand, the transfer function $r(a, w;\xi)$ strongly depends on both wavelength and visibility and is therefore crucial for the air-water interface correction.

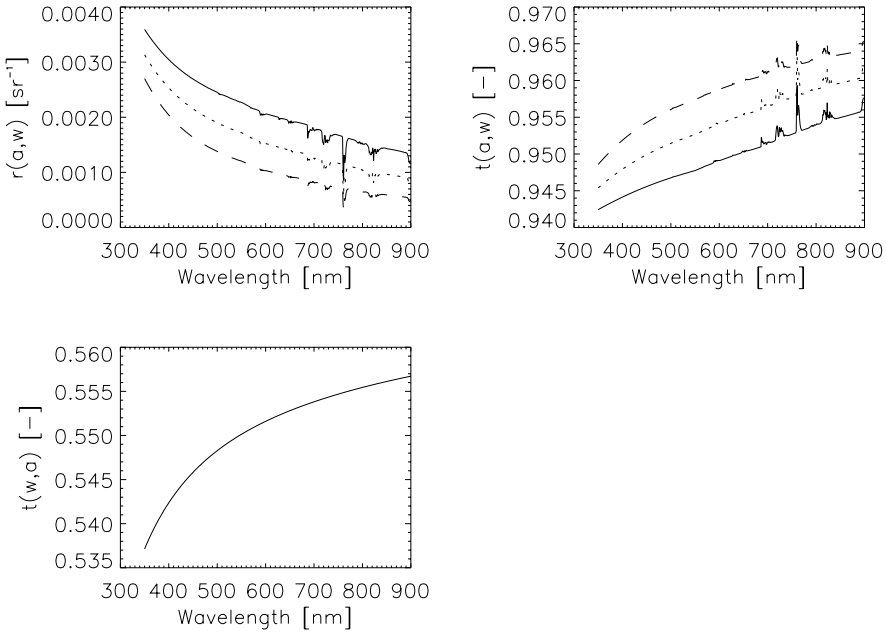

Figure 1 Transfer functions calculated for variable visibilities (solid: 5 km, dotted: 10 km, dashed: 20 km).

2. 3 Determination of the Visibility

One important parameter for the atmospheric and the interface correction is the visibility (*VIS*) and accurate and objective methods are needed for its determination. Values are obtained by measurements in combination with atmospheric radiative transfer models; sun photometer or image data can be applied for this purpose.

Image-Based Method

The image-based method developed in this study merely allows the determination of the visibility, whereas the atmospheric and aerosol model are considered to be known from the sun photometer measurements or are determined by an educated guess.

It is presumed that the water-leaving reflectance in the near-infrared is negligible and that therefore Eq. 4 can be simplified to:

$$R_{Rs}(a;\xi) = r(a, w;\xi) \text{ [sr}^{-1}\text{]}. \tag{5}$$

The equation states that the remote sensing reflectance is equal to the surface reflection and therefore independent of the water constituents and only dependent on atmospheric parameters. Both parameters are determined for visibilities of 5, 10, 20, 30, and 50 km. The optimal parameter set for the atmospheric correction fulfils Eq. 5.

In case of high suspended matter concentration or incorrect glitter correction, the algorithm has to be extended. To take account of this, first the visibility and the corresponding reflectance in the near infrared for each pixel are calculated with the dark target assumption. Then the minimum reflectance

of a certain area around each pixel is determined. In this area at least one pixel should exist with small sediment concentration and no glint effect; on the other hand, the atmospheric parameters are assumed to be constant. The corresponding visibility of the pixel with the minimum reflectance is associated to the central pixel. In this study, the filter width was set equal to 50 pixels.

Sun Photometer Method

The direct transmittance can be calculated with the visibility as a variable input parameter for given geometric conditions and atmospheric and aerosol models. The modelled values are compared with measured values, enabling a direct determination of the visibility. For the field measurements, a Reagan sun photometer is used (Ehsani and Reagan, 1992).

2. 4 Determination of Chlorophyll a

Almost all semi-analytical inversion algorithms are based on the single-scattering approximation. Gordon et al. (1988) use the form:

$$\frac{R(\lambda)}{Q(\lambda;\xi)} = f_1\omega(\lambda) + f_2\omega^2(\lambda)\ [\mathrm{sr}^{-1}], \tag{6}$$

where

$$\omega(\lambda) = \frac{b_b(\lambda)}{b_b(\lambda) + a(\lambda)}\ [-] \tag{7}$$

is the single scattering coefficient, Q [sr] the ratio of the upwelling irradiance to the upwelling radiance pointing into the viewing direction ξ, $f_1 = 0.0949$ sr^{-1} and $f_2 = 0.0794$ sr^{-1}. The approximation is based on the fact that the scattering phase function is strongly peaked in the forward direction – most photons are not backscattered relative to the incident beam and hence remain in the beam. The approximation is better than 10% for common phase functions for sun zenith angles greater than 20° (Gordon et al., 1988). A limitation of this approximation is that the influence of the vertical distribution, bottom effects, and fluorescence are not integrated.

The approximation can be rewritten as a linear equation system for the desired water constituents (Hoge and Lyon, 1996; Vasilkov, 1997; Keller et al., 1998). The equation system depends on the assumption made for absorption and scattering. For example, if we define:

$$a(\lambda) = a_w(\lambda) + a_g(\lambda) + CHL \cdot a_p^*(\lambda), \tag{8}$$

and

$$b_b(\lambda) = b_{b,w}(\lambda) + CHL \cdot b_{b,org}^*(\lambda) + b_{b,inorg}(\lambda), \tag{9}$$

we obtain an equation system for CHL and $b_{b,inorg}$:

$$\begin{aligned} CHL\{\omega(\lambda)[a_p^*(\lambda) + b^*_{b,org}(\lambda)] - b^*_{b,org}(\lambda)\} + b_{b,inorg}\{\omega(\lambda) - 1\} \\ = b_{b,w}(\lambda) - \omega(\lambda)[b_{b,w}(\lambda) + a_w(\lambda) + a_g(\lambda)] \end{aligned} \tag{10}$$

If more than two bands are used, Eq. 10 becomes an overdetermined equation system (i.e., one equation for each band) which can be solved using least square matrix inversion techniques (Press et al., 1992). The form of Eq. 10 is not unique, but has been chosen, because it results into the most stable results. Especially the inverse of $\omega(\lambda)$ has been omitted, since the weighting of small values would increase in the inversion which leads to unsatisfying results.

Water absorption in the spectral range 400-700 nm is taken from Pope and Fry (1997), in the range 700-800 nm from Palmer and Williams (1974). The absorption of gelbstoff a_g is assumed to be proportional to the concentration of the total dissolved organic carbonates (*DOC*) with an exponential spectral dependency:

$$a_g(\lambda) = DOC \times a_g^*(440\text{nm}) \times e^{-S(\lambda - 440\,nm)}\ [\text{m}^{-1}], \tag{11}$$

where DOC [μg l^{-1}] x $a_g^*(440\text{nm})$ [l μg^{-1}] is equal to the gelbstoff absorption at 440 nm. The parameters S and $a_g^*(440\text{nm})$ are taken to be equal to the values measured in Lake Zurich (unpublished data), a lake situated 15 km to the north of Lake Zug with similar properties: $a_g^*(440\text{nm})$ = 0.019 l mg^{-1}, S = 0.027 nm^{-1}. Because the in situ determination of *DOC* only showed little variation in the lake (2.6 ± 0.2 mg l^{-1}), the gelbstoff absorption was set constant for further calculations.

The absorption of the photosynthetic active pigments is given by:

$$a_{phyto}(\lambda) = CHL \times a^*_{phyto}(\lambda)\ [\text{m}^{-1}], \tag{12}$$

where a^*_{phyto} is the specific algae absorption spectrum. For this study, an average spectrum of Lake Constance (Gege, 1994) is used.

The specific backscattering coefficients for organic particulate matter ($b_{b,\,inorg}(\lambda)$) are determined using *in situ* radiometric measurements.

2. 5 Remote Sensing Data

The sensor specifications and atmospheric model parameters are listed in Table 1.

Table 1 CASI specification and model parameters.

Centre Wavelength [nm]	499, 518, 542, 567, 587, 603, 621, 639, 654, 671, 688, 705,722, 739, 753, 767, 860, 900, 944
Full width at half maximum [nm]	17, 21, 28, 21, 21, 12, 25,, 12, 17, 18, 17, 18, 18, 16, 14, 16, 21, 14, 14
Ground altitude of lake surface	414 m above sea level
Flight altitude	4150 m above sea level
Ground resolution	5 m
Date	August 10, 1997
Flight heading	South to North
Sun azimuth / zenith angle	135° E / 48 °
Atmosphere	Mid-altitude summer

3. Results

3. 1 Visibility Map

Fig. 2 shows all steps for the generation for the visibility map and the resulting maps for rural and

urban aerosols, respectively. The distribution is similar. However, the absolute quantities differ strongly which also affects the visibility near the position of the sun photometer that is 32 km for rural aerosols, and 20 km for urban aerosols.

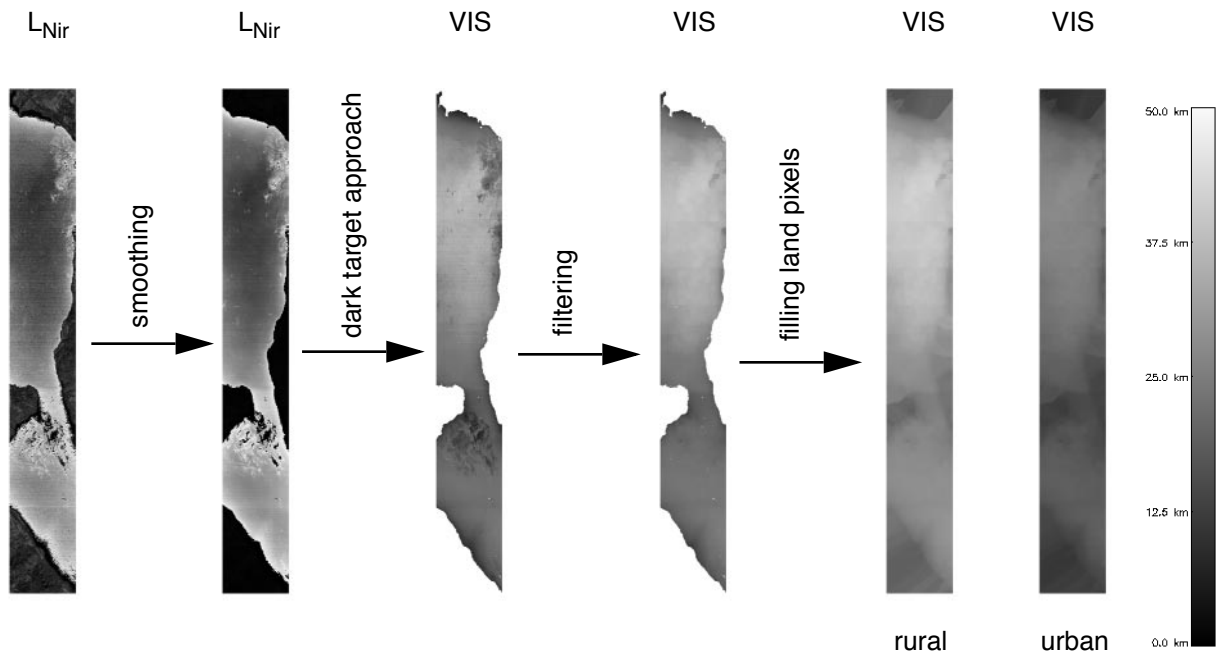

Figure 2 Necessary steps for the generation of the visibility map. First, a near infrared band is chosen and filtered in order to avoid unrealistic variations. Then, the visibility for all water pixels is calculated based on the dark target approach. This map has to be filtered again due to glitter effects or influences of high sediment concentrations. Finally, the visibility is calculated for the land pixels using nearest neighbor interpolation. The resulting visibility map is shown for rural and urban aerosols.

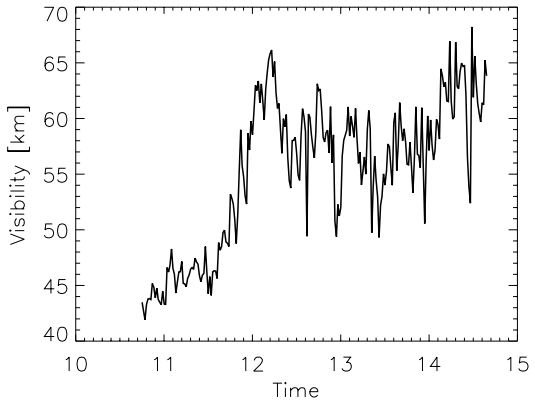

Figure 3 Visibility retrieved using the sun photometer as a function of day time.

Fig. 3 shows the retrieved visibility using the sun photometer method for comparison. The instrument was situated at the harbour of Zug on the northern shore of the lake. Long time trends and short time changes in the order of minutes are observable. Unfortunately, the flight was performed before

the first acquisition of the sun photometer data. However, the visibility during the overflight at 10:38 a.m. can be guessed with linear extrapolation to a value of 41 km, which is higher than the image-based values. But as the temporal changes are high and this discrepancy may only be introduced by a wrong extrapolation, and as relative changes of the visibility over 30 km do not strongly affect the model quantities anymore, the result is satisfying.

3. 2 Chlorophyll a Map

Chlorophyll maps (Fig. 4) were calculated for image-based visibility maps shown in Fig. 2 and for constant visibilities for the whole scene (15, 30 km) and two different aerosol models (rural, urban).

The horizontal variations and the absolute quantities differ strongly between the different case studies especially for constant visibility. The image-based method allows to decrease the influence of the aerosol models. However, the influence of adjacency effects near the lake border are enforced since these effects are pronounced in the near infrared due to high reflectances differences between lake and land vegetation. Regions with high reflectances caused by surface glitter or high particulate matter concentration may lead to negative values; this is supposed to be an artefact of the inversion method or due to ill-chosen inherent parameters.

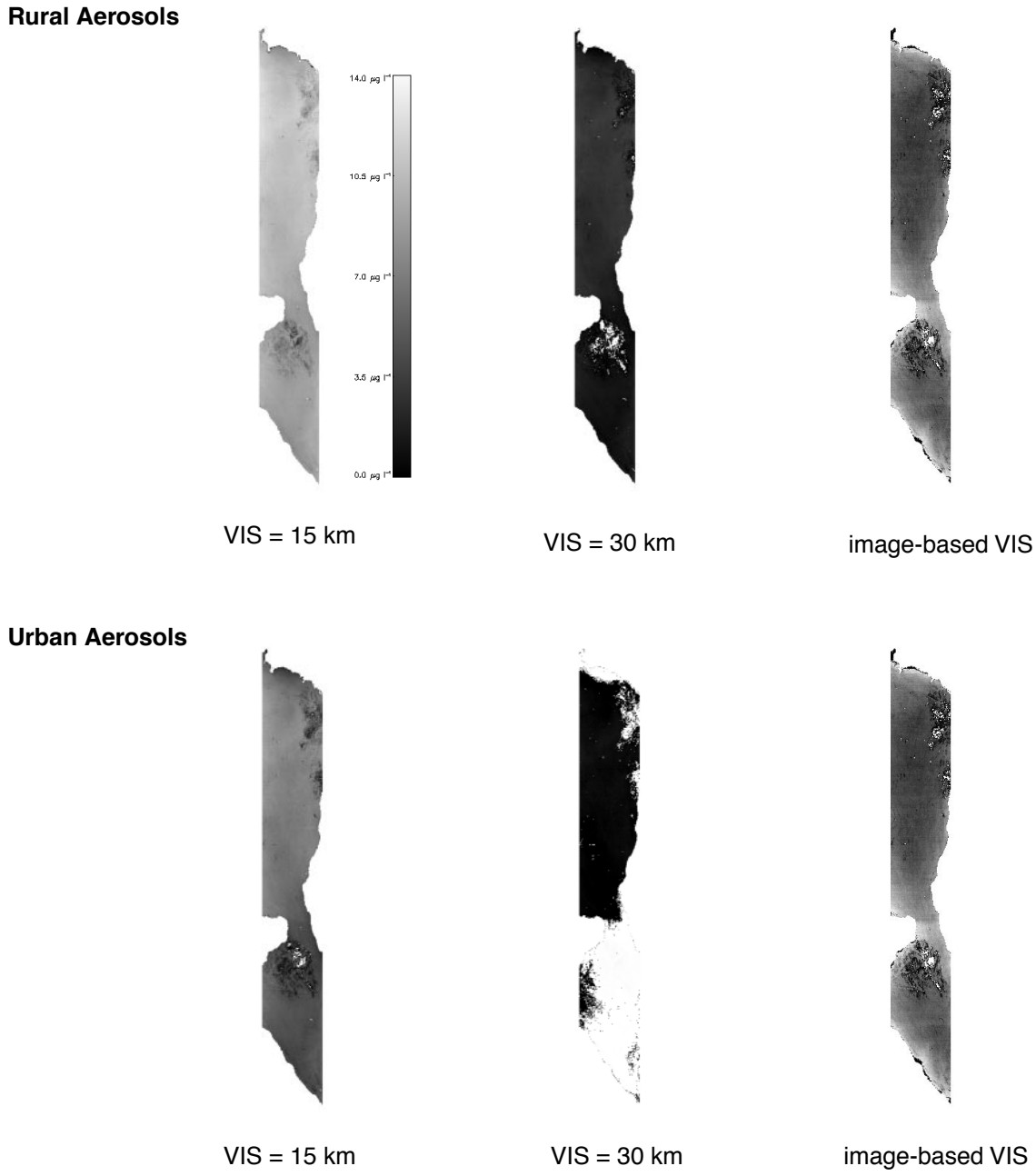

Figure 4 Chlorophyll maps based on the visibility map in Fig. 2 and for constant visibilities (15, 30 km) and two different aerosol models (rural, urban).

It is interesting to see that the image-based visibility map leads to less variations than obtained with constant visibilities (Fig. 5). During the campaign, in situ measurements of *CHL* have been performed at eight stations (Fig. 6). Of course, the quality of the results does not only depend on the pre-correction, but also on the bio-optical model and the inherent optical properties used for the inversion. The variations between the different case studies are higher then the inter-scene variations which indicates the importance of a reliable pre-correction.

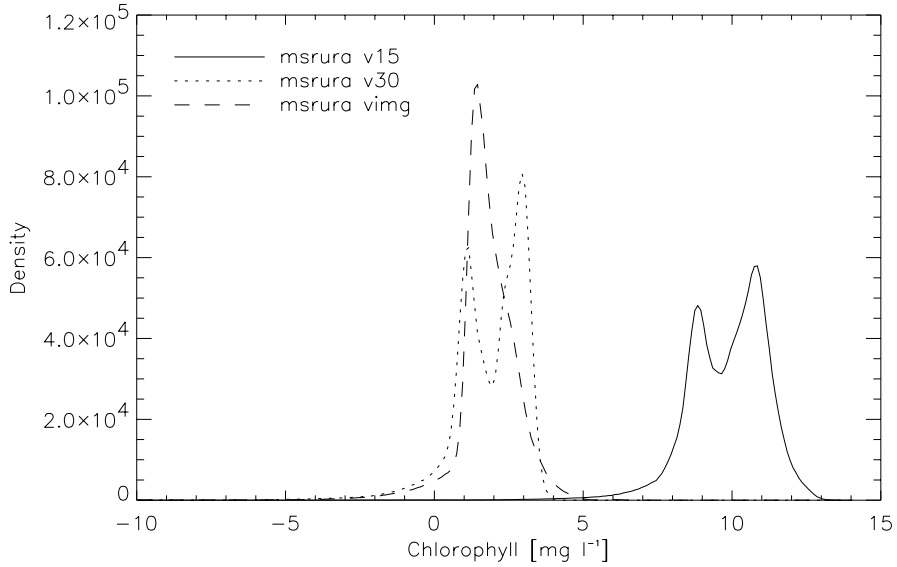

Figure 5 Frequency distribution of the chlorophyll maps using rural aerosols. The inter-lake variations disappear with the image-based method.

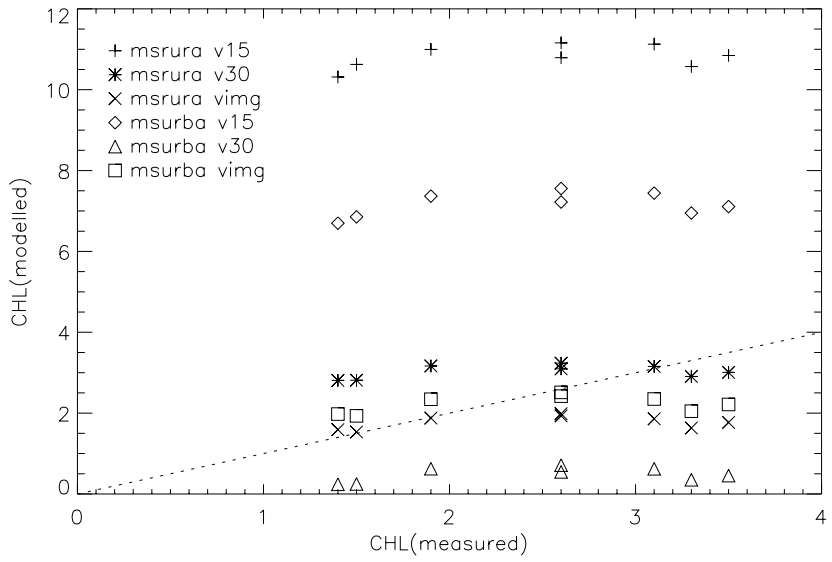

Figure 6 Measured versus modelled chlorophyll concentrations for the different case studies.

4. Discussion

The most important lessons learnt in this study are:

- the results of the image-based method are encouraging,
- the image-based retrieval of the visibility allows the investigation of the horizontal variation of an atmospheric parameters (i.e., the visibility),
- the image-based retrieval of the visibility leads to less variations in the chlorophyll concentrations which may be an artefact introduced by the method,
- adjacency effects become visible due to the dependency of the visibility on the near infrared band,
- the atmospheric model parameter have a strong impact on the retrieved chlorophyll maps,
- the sensor requirements especially in the near infrared is high, and
- the influences of glitter effects, high sediment concentration and changing atmospheric conditions can hardly be separated and will be investigated in further studies.

5. Acknowledgement

The CASI flight was performed with help of I. Keller (Free University of Berlin). The limnological measurements have been performed with help of S. Meyns, D. Kobler, C. Stengel, I. Baur (EAWAG), R. Beck (Kanton Zug), P. Müller (RSL), and F. Schanz (Limnological Station, University of Zurich). ATCOR 4 was provided by R. Richter (DLR). This work has been carried out under the support of the Swiss National Science Foundation (contract-no. 20-50727.97).

6. References

Berk A., Bernstein L. S., and Robertson D. C, 1989. MODTRAN: a moderate resolution model for LOWTRAN 7. *GL-TR.89-0122, U.S. Air Force Geophysics Laboratory, Hanscom Air Force Base, Mass*.

Bukata R. P. , Jerome J. H., Kondratyev K. Y., and Pozdnyakov D.V., 1995. Optical Properties and Remote Sensing of Inland and Coastal Waters. *CRC Press, Boca Raton*, 362 pp.

Ehsani A. R., and Reagan J. A., 1992. A Microprocessor Based Auto Sun-Tracking Multi-Channel Solar Radiometer System. In *Proceedings of IGARSS'92*, Houston, TX, 1696-1698.

Gege P., 1994. Gewässeranalyse mit passiver Fernerkundung: Ein Modell zur Interpretation optischer Spektralmessungen. *DLR Forschungsbericht*, 94-15, 171 pp.

Gordon H. R., Brown O. B., Evans R. H., Brown J. W., Smith R. C., Baker K. S., and Clark D. K., 1988. A semianalytic radiance model of ocean color. *J. Geophys. Res.* 93: 10,909-10,924.

Hoge F. E., and Lyon P. E., 1996. Satellite retrieval of inherent optical properties by linear matrix inversion of oceanic radiance models: an analysis of model and radiance measurement errors. *J. Geophys. Res.* 101: 16,631 – 16,648.

Kaufman Y. J., and Sendra C., 1988. Algorithm for automatic atmospheric corrections to visible and near-IR satellite imagery. *Int. J. Remote Sensing*, 9: 1357-1381.

Keller P., Keller I., and Itten K. Combined Hyperspectral Data Analysis of an Alpine Lake Using CASI and DAIS 7915 Imagery. *1st EARSeL Workshop on Imaging Spectroscopy, 6-8 October 1998, Zurich, Switzerland, EARSEL, Paris, 1998*, pp. 237-243.

Palmer K. F., and Williams D. J., 1974. Optical properties of water in the near infrared. *Appl. Opt.* 64(2): 1107-1110.

Pope R. M., and Fry E. S., 1997. Absorption spectrum (380-700 nm) of pure water. II. Integrating cavity measurements. *Appl. Opt.* 36(33): 8710-8723.

Press W. H., Teukolsky S. A., Vetterling W. T., and Flannery B.P., 1988. Numerical Recipes in C. *Cambridge University Press, Cambridge*, 994 pp.

Richter R., 1999. Amospheric/Topographic correction for wide FOV airborne imagery: model Atcor 4, Version 2.0, *DLR Report DLR-IB 552-05/99, German Aerospace Center, Institute for Optoelectronics*.

Vasilkov A. P., 1997. A retrieval of coastal water constituent concentration by least-squares inversion of a radiance model. *Proceedings of the Fourth International Conference on Remote Sensing for Marine and Coastal Environments, Orlando, Florida, 17-19 March*, pp. II-107–II-115.